ARTICLES

Miscible droplets in a porous medium and the effects of Korteweg stresses

Ching-Yao Chen and Lilin Wang
Department of Mechanical Engineering, Da-Yeh University, Chang-Hwa, Taiwan, Republic of China

Eckart Meiburg[a)]
Department of Mechanical and Environmental Engineering, University of California at Santa Barbara, Santa Barbara, California 93106

(Received 6 December 2000; accepted 16 May 2001)

Numerical simulation results are presented for the displacement of a drop in a porous medium. The drop is surrounded by a more viscous fluid with which it is fully miscible. The simulations are based on a set of augmented Hele–Shaw equations that account for nonconventional, so-called Korteweg stresses resulting from locally steep concentration gradients. Globally, these stresses tend to stabilize the displacement. However, there are important distinctions between their action and the effects of surface tension in an immiscible flow. Since the Korteweg stresses depend on the concentration gradient field, the effective net force across the miscible interface region is not just a function of the drop's geometry, but also of the velocity gradient tensor. Locally high strain at the leading edge of the drop generates steep concentration gradients and large Korteweg stresses. Around the rear of the drop, the diffusion layer is much thicker and the related stresses smaller. The drop is seen to form a tail, which can be explained based on a pressure balance argument similar to the one invoked to explain tail formation in Hele–Shaw flows with surfactant. The dependence of such flows on the Peclet number is complex, as steeper concentration gradients amplify the growth of the viscous fingering instability, while simultaneously generating larger stabilizing Korteweg forces. © *2001 American Institute of Physics.* [DOI: 10.1063/1.1387468]

I. INTRODUCTION

The displacement of a drop of one fluid surrounded by a different fluid in a porous environment represents a problem of fundamental interest. At the same time, it is of importance in a variety of environmental as well as technological situations ranging from groundwater contamination and enhanced oil recovery to biomedical applications. Much of the research in this area has exploited the analogy between displacements in true porous media and those in Hele–Shaw cells, as described in the reviews provided by Homsy,[1] Yortsos,[2] as well as McCloud and Maher.[3] With regard to the motion of drops and bubbles in Hele–Shaw flows, it appears that *immiscible* displacements have received far more attention than *miscible* ones, see the experimental investigations by Eck and Siekmann,[4] Maxworthy,[5] Kopf-Sill and Homsy,[6] as well as Park *et al.*[7] The observations by these authors demonstrate that the combination of viscous and surface tension forces in conjunction with three-dimensional effects can lead to a variety of striking and unexpected shapes.

These findings in turn stimulated theoretical efforts to explain, as a function of the dimensionless surface tension parameter and the bubble size, both the multitude of experimentally observed and numerically computed steady bubble shapes (Tanveer[8,9]), as well as their stability properties (Tanveer and Saffman[10]) on the basis of the Hele–Shaw equations. These authors were able to demonstrate that surface tension removes the degeneracy of the earlier Taylor–Saffman zero surface tension solutions (Taylor and Saffman[11]). Tanveer observed that for larger bubbles, the leading front tends towards the solutions found by McLean and Saffman[12] for fingers. A second branch exhibits nearly circular bubbles for small, and flattened bubbles for larger surface tension values. Interestingly, for a certain bubble size of about one quarter of the cell width, he finds an extraordinary, or Tanveer, shape with negative curvature at the leading front. A wide range of propagation velocities is observed, however all of them are faster than the velocity of the surrounding fluid. Thus some, but not all of the shapes found experimentally by Kopf-Sill and Homsy are explained. These authors record six types of bubble shapes, termed near circles, flattened, elongated, long-tail, short-tail, and Tanveer bubbles, with propagation velocities ranging from one fifth to twice that of the surrounding fluid. The follow-up work by Park *et al.*[7] suggests that surfactant contamination may have played a role in some of the shapes observed by Kopf-Sill and Homsy. In the absence of surfactant effects, they exclusively find bubble velocities larger than that of the surrounding fluid. In the presence of surfactants, on the other hand, very small bubble velocities and shapes similar to those found by Kopf-Sill and Homsy are observed. Park *et al.* ar-

a)Author to whom all correspondence should be addressed; electronic mail: meiburg@engineering.ucsb.edu

gue that if the bubble moves more slowly that the fluid, surfactant accumulates at the front and locally lowers the surface tension. In order to balance the pressure forces acting on the bubble, an elongated shape with a more strongly curved tip must form. A corresponding argument applies to the formation of the ''tailed bubble,'' if the bubble velocity is greater than that of the fluid. At the same time, three-dimensional effects are also known to be important for the motion of bubbles and droplets in tubes and Hele–Shaw cells, see Bretherton[13] as well as Park and Homsy.[14] However, by themselves they cannot explain the multitude of shapes observed by Kopf-Sill and Homsy (Meiburg[15]).

The above results for immiscible displacements are of renewed interest in light of recent findings regarding the effects of nonconventional stresses in *miscible* fluid flows with steep concentration gradients. Such stresses were first postulated by Korteweg[16] who, on the basis of an *ad hoc* constitutive equation, suggested that they may result in dynamic surface tension-like effects, or an ''effective surface tension.'' More recently, experimental observations by Joseph[17] rekindled interest in Korteweg's original work and stimulated a host of further research in this area. Joseph found that drops of water rising in glycerine exhibit sharp interfaces and are characterized by shapes that resemble those commonly seen in immiscible flows. Already several years earlier, Kojima *et al.*[18] had found that the behavior of toroidal drops falling in a surrounding liquid could be predicted by theoretical arguments only under the assumption of a small, time-dependent interfacial tension across the drop interface. The work of Joseph and coauthors also drew attention to the fact that the velocity field of a miscible fluid flow may not be solenoidal, even if the fluids are incompressible. Further examples that highlight and discuss these effects are provided by Galdi *et al.*,[19] Joseph and Renardy,[20] and Joseph *et al.*[21]

Over the years, there have been numerous attempts to obtain dynamic surface tension values. Quinke,[22] as cited by Freundlich,[23] measured the dynamic tension of ethyl alcohol with a salt solution. He observed the value to lie between 0.8 and 3×10^{-3} N/m. Smith *et al.*[24] reported a maximum surface tension value of 10^{-3} N/m at the time of initial contact between silicone oils of 1 and 2000 cSt. Comparison between the miscible capillary tube experiments of Petitjeans and Maxworthy[25] and earlier immiscible experiments by Taylor[26] suggests an effective surface tension value between glycerine and water of about 0.5×10^{-3} N/m, see also the corresponding numerical work by Chen and Meiburg.[27] Subsequent simulations of miscible capillary flows by Chen and Meiburg[28] that account for Korteweg stresses, show that a negative stress constant can substantially slow down the less viscous finger that travels along the centerline of the tube. Based on theoretical arguments, Davis[29] calculates values for mixtures of hydrocarbons up to 10^{-4} N/m. Similar effects were observed by Kurowski and Misbah,[30] Petitjeans,[31] as well as Petitjeans and Kurowski.[32]

Hu and Joseph[33] consider effective surface tension and divergence effects for miscible displacements in a Hele–Shaw cell. These authors formulate gap averaged equations that account for both of these phenomena, and they subsequently perform a linear stability analysis for a rectilinear front. Fernandez *et al.*[34] perform comparisons between experiments and three-dimensional direct numerical simulations of the density driven instability between miscible fluids in vertical Hele–Shaw cells, in order to identify effective surface tension effects.

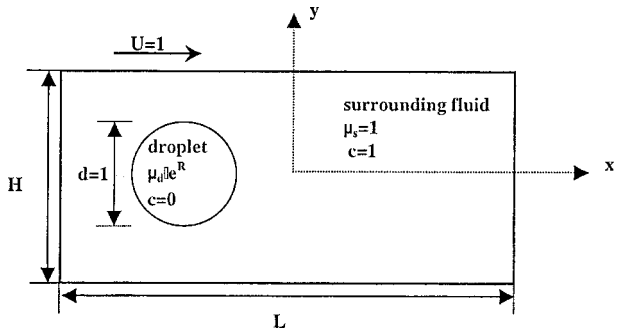

FIG. 1. Principal sketch. In a rectangular domain, an initially circular droplet is displaced by a surrounding fluid of different viscosity.

As the above references show, there is substantial evidence that miscible flows can give rise to stresses that are not accounted for by the model of a Newtonian fluid. At the same time, the physical and mathematical nature of these stresses, as well as their magnitude and even their sign, are still poorly understood. There are suggestions, most notably by Joseph and coauthors, regarding the mathematical form of additional stress terms to be incorporated into the Navier–Stokes equations, in order to account for Korteweg forces. While those terms have been proposed on somewhat empirical grounds, and a derivation from first principles is not yet available, they nevertheless open up new avenues for investigating these nonconventional stresses. It appears worthwhile to conduct careful numerical simulations based on the proposed augmented equations against which corresponding experiments can be compared, in order to establish or disprove the validity of the additional terms. Furthermore, the mechanisms by which the proposed additional stress terms influence the flow can be analyzed by means of the numerical simulations as well. Miscible droplets in a Hele–Shaw displacement represent a highly suitable focus for such an investigation, as surface tension forces are known to give rise to very pronounced effects in their immiscible equivalents, which have been studied in great detail. This, in conjunction with the importance of miscible porous media flows in their own right, is the motivation behind the simulations to be discussed below.

The presentation is structured as follows. The physical problem will be setup in Sec. II, along with the governing equations and the computational technique. In Sec. III, we will establish and interpret the flow features as function of the governing dimensionless control parameters, such as the flow rate, viscosity ratio, and Korteweg stress constant. Finally, Sec. IV will provide a discussion of the results, as well as some conclusions.

II. PHYSICAL PROBLEM AND GOVERNING EQUATIONS

Consider the time-dependent displacement of an incompressible miscible drop by a uniform Hele–Shaw flow of finite lateral extent (Fig. 1). Hu and Joseph[33] propose exten-

sions to Darcy's law that account for velocity divergence effects as well as dynamic Korteweg stresses in a homogeneous porous medium of permeability k. Thus, the governing equations take the form

$$\nabla\cdot\left(\mathbf{u}-\frac{\xi D}{1-\xi c}\nabla c\right)=0, \tag{1}$$

$$\nabla[p+Q(c)]=-\frac{\mu}{k}\mathbf{u}+\nabla\cdot[\hat{\delta}(\nabla c)(\nabla c)^T], \tag{2}$$

$$Q(c)=\frac{\hat{\delta}}{3}\left[\left(\frac{\partial c}{\partial x}\right)^2+\left(\frac{\partial c}{\partial y}\right)^2\right]+\frac{2\gamma}{3}\left(\frac{\partial^2 c}{\partial x^2}+\frac{\partial^2 c}{\partial y^2}\right)+\frac{2\xi\mu}{3}\left[\frac{\partial}{\partial x}\left(\frac{D}{1-\xi c}\frac{\partial c}{\partial x}\right)+\frac{\partial}{\partial y}\left(\frac{D}{1-\xi c}\frac{\partial c}{\partial y}\right)\right], \tag{3}$$

$$\frac{\partial c}{\partial t}+\nabla\cdot(\mathbf{u}c)=\nabla\cdot\left(\frac{D}{1-\xi c}\nabla c\right). \tag{4}$$

Here $\mathbf{u}$ denotes the velocity, c the concentration of the surrounding fluid, and ξ is the normalized density difference of the two fluids

$$\xi=\frac{\rho_s-\rho_d}{\rho_s}, \tag{5}$$

where the subscripts s and d denote the surrounding and droplet fluids, respectively. D represents the diffusion coefficient, p the pressure, μ the viscosity, and Q indicates the additional pressure due to the Korteweg stresses. $\hat{\delta}$ and γ denote the two Korteweg stress coefficients, which in the following are assumed to be constant. As mentioned above, only rough estimates exist as far as the magnitude of $\hat{\delta}$ and γ is concerned, and even their respective signs are unknown. Consequently, we will have to vary these coefficients in the simulations, in order to assess their influence on the drop displacements. The above set of equations expresses the conservation of mass, momentum, and species. Here, the assumption of a constant, scalar diffusion coefficient D represents a relatively crude approximation of the true mechanisms responsible for dispersion in a porous medium, or even in a Hele–Shaw cell, cf. the discussion and references given by Petitjeans *et al.*[35] Nevertheless, for lack of a better model we employ this approach here.

In order to render the governing equations dimensionless, we take the droplet diameter d as the characteristic length scale, and k as a typical permeability value. The nominal displacement velocity U of the surrounding fluid serves as the velocity scale, thereby providing us with characteristic values of time, d/U, and pressure, $\mu_s Ud/k$. We furthermore scale viscosity with μ_s and assume a viscosity-concentration relationship of the form (Tan and Homsy,[36] Chen and Meiburg[37,38])

$$\mu(c)=e^{R(1-c)}. \tag{6}$$

By introducing the solenoidal velocity $\mathbf{W}$, we can recast the momentum equation into a vorticity (ω) and streamfunction (ψ) formulation (Ruith and Meiburg,[39] Camhi *et al.*[40]):

$$\mathbf{W}=\mathbf{u}-\frac{\xi D}{1-\xi c}\nabla c, \tag{7}$$

$$\omega=\frac{\partial W_y}{\partial x}-\frac{\partial W_x}{\partial y}, \tag{8}$$

$$W_x=\frac{\partial\psi}{\partial y},\quad W_y=-\frac{\partial\psi}{\partial x}, \tag{9}$$

so that we obtain

$$\nabla^2\psi=-\omega, \tag{10}$$

$$\omega=-R\nabla\psi\cdot\nabla c+\frac{\delta}{\mu}\left[\frac{\partial c}{\partial x}\left(\frac{\partial^3 c}{\partial x^2\partial y}+\frac{\partial^3 c}{\partial y^3}\right)-\frac{\partial c}{\partial y}\left(\frac{\partial^3 c}{\partial x\partial y^2}+\frac{\partial^3 c}{\partial x^3}\right)\right], \tag{11}$$

$$\frac{\partial c}{\partial t}+\mathbf{W}\cdot\nabla c=\frac{1}{\mathrm{Pe}}\nabla^2 c. \tag{12}$$

Here the Peclet number Pe and the dimensionless Korteweg constant δ are of the form

$$\mathrm{Pe}=\frac{Ud}{D},\quad \delta=\frac{k\hat{\delta}}{\mu_s Ud^3}. \tag{13}$$

Note that as a result of employing the stream function-vorticity formulation, the additional pressure component Q, and with it the second Korteweg stress constant γ are eliminated, so that δ is the only additional parameter resulting from the nonconventional stress terms.

Boundary conditions are prescribed as follows (Ruith and Meiburg,[39] Camhi *et al.*[40]):

$$x=\pm\frac{L}{2}:\quad \frac{\partial\psi}{\partial x}=0,\ \frac{\partial\omega}{\partial x}=0,\ \frac{\partial c}{\partial x}=0, \tag{14}$$

$$y=\pm\frac{H}{2}:\quad \psi=\pm\frac{H}{2},\ \frac{\partial c}{\partial y}=0. \tag{15}$$

The initial conditions assume a circular droplet shape bounded by a steep concentration gradient. Both c, ω, and ψ are expanded in a cosine series in the streamwise direction. In the normal direction, discretization is accomplished by sixth order compact finite differences (Lele[41]). Time integration is fully explicit and utilizes a third order Runge–Kutta procedure (Wray[42]). The evaluation of the nonlinearity at each time level is performed in a pseudospectral manner (Canuto *et al.*[43]). The simulations to be discussed below typically employ a discretization of $\Delta x=\Delta y=\frac{1}{128}$, except for the cases of the highest viscosity ratio and Peclet number, where we use $\Delta x=\Delta y=\frac{1}{256}$. The results have been validated by grid refinement tests. The numerical code is largely identical to one used earlier for investigating planar fronts (Ruith and Meiburg,[39] Camhi *et al.*[40]), which had been validated by comparing growth rates of small perturbations with linear stability results. More detailed information on the implementation is provided by Meiburg and Chen[44] as well as Ruith and Meiburg.[39]

III. RESULTS

We begin by describing a reference case, in order to identify the mechanisms that dominate the temporal and spatial evolution of the displacement. Subsequently, the values of the governing parameters will be varied individually.

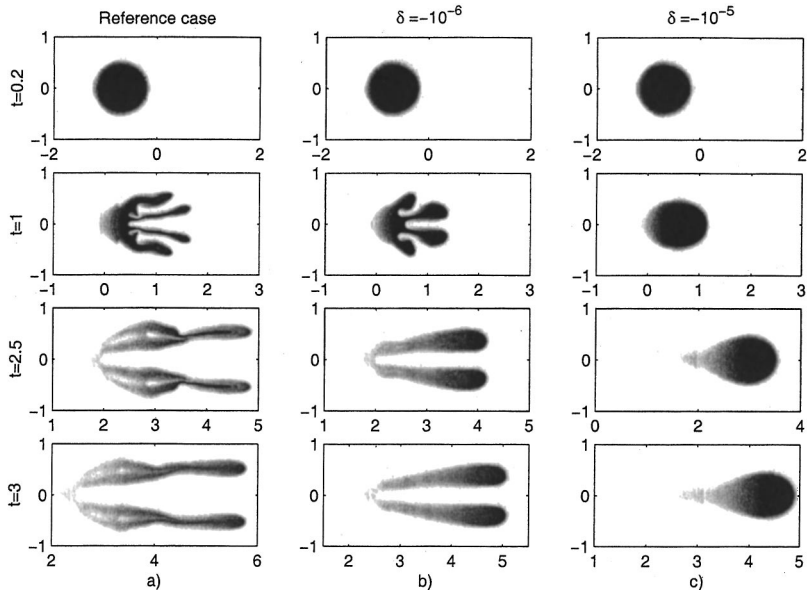

FIG. 2. Pe=2000, $R=-2.5$, and (a) $\delta=0$, (b) $\delta=-10^{-6}$, (c) $\delta=-10^{-5}$. Concentration contours are shown for times $t=0.2$, 1, 2.5, and 3. (a) Reference case: In the absence of Korteweg stresses, a fingering instability develops. The long-time evolution of the flow is characterized by a pair of a decaying fingers. (b) Small Korteweg stresses lead to slower growth and fewer fingers overall, without stabilizing the droplet completely. (c) Larger Korteweg stresses suppress viscous fingering entirely.

A. Reference case

Figure 2(a) depicts the motion of a droplet for $R=-2.5$, Pe=2000, and $H=2$ in the absence of Korteweg stresses. The computational domain extends over the range $(-2,6)$, and the droplet is initially centered at $(-1,0)$. The R value indicates that the droplet is moving within an environment that is approximately 12 times more viscous. This viscosity ratio results in a locally unstable situation at the front of the drop, where the growth of a vigorous fingering instability is observed. In the absence of symmetry breaking perturbations, the droplet remains symmetrical with respect to the center line, with matching pairs of fingers forming on each side. These fingers initially display some of the dynamic behavior familiar from investigations of nominally plane fronts, such as merging and shielding, cf. Tan and Homsy.[36] Due to the finite supply of the less viscous fluid, however, the long time behavior is characterized by the propagation of a pair of fading fingers. This evolution is also reflected by the corresponding streamfunction and vorticity data (Fig. 3). While initially substantial fine scale structure exists, the long term evolution displays two fairly uniform channels along which most of the droplet fluid transport

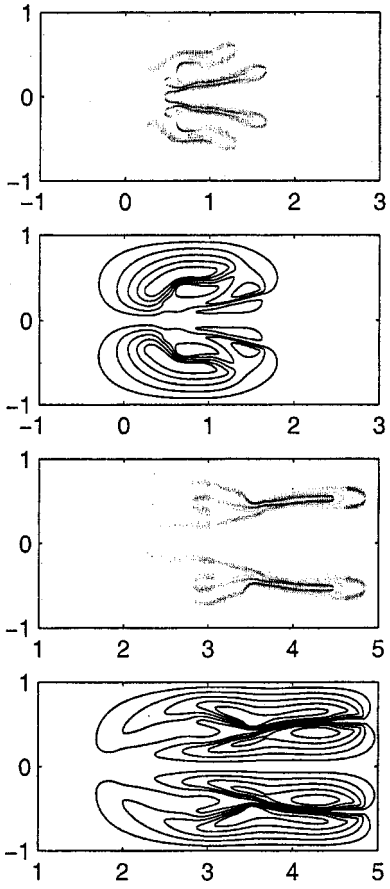

FIG. 3. Reference case: Vorticity and perturbation stream function fields at times $t=1$ and 2.5.

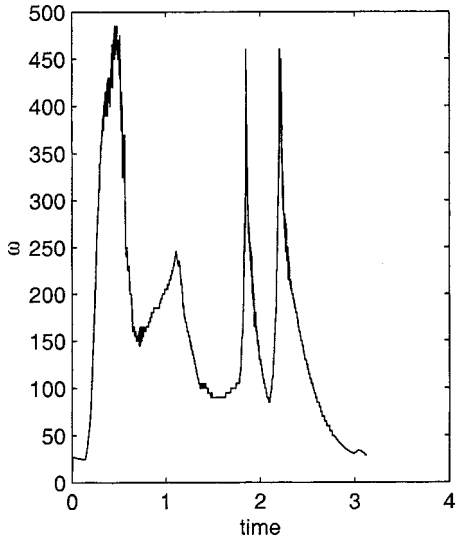

FIG. 4. Reference case: Maximum absolute vorticity as a function of time. After an initial transient, the vorticity maximum grows rapidly, which reflects the growth of the viscous fingering instability at the leading edge. For long times, saturation occurs as a result of nonlinear effects.

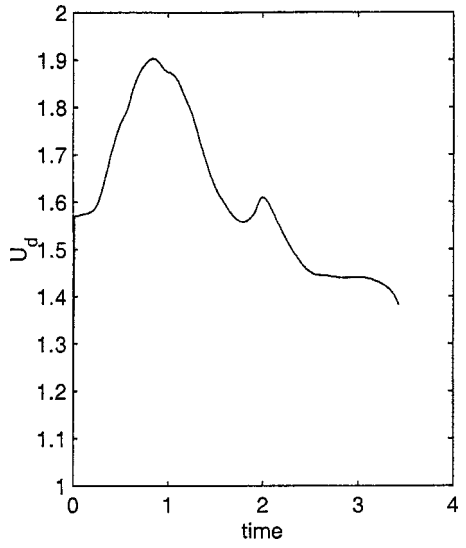

FIG. 5. Reference case: The temporal evolution of the weighted velocity U_d. Initially it increases sharply to a maximum of about 1.9, thereafter it declines.

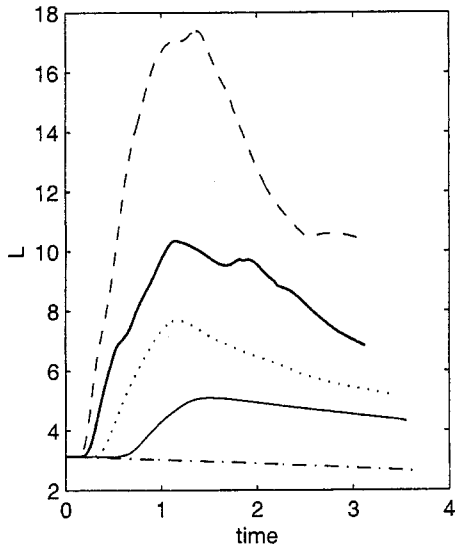

FIG. 6. Temporal evolution of the interfacial length $L(t)$ for Pe=200 (dash–dot), 500 (solid), 1000 (dot), 2000 (bold), 4000 (dash). $L(t)$ increases with Pe, reflecting the destabilizing influence of Pe in the absence of Korteweg stresses.

takes place. Figure 4 shows the growth of the maximum absolute vorticity value in the flow field. After a brief initial transient during which the droplet deforms slightly from its original circular shape, the vorticity shows a distinct time interval of sharp growth, which reflects the emergence of several pairs of vorticity dipoles near the drop's tip, where subsequently the formation of fingers is triggered. As these fingers evolve, large vorticity peaks appear in regions where mergings take place. At the same time, the overall growth becomes saturated. Very little vorticity emerges in the stable region near the rear of the droplet.

The overall droplet propagation velocity U_d represents a quantity of significant practical interest. Kopf-Sill and Homsy[6] as well as Park *et al.*[7] measure the steady state propagation velocities of immiscible bubbles in different parameter ranges, and they report values for U_d between 0.2 and 2. For the current, miscible drops, a steady state does not evolve. As a result, it is most appropriate to define an instantaneous mass-weighted droplet velocity U_d as

$$U_d(t)=\frac{\int\int W_x c\,dx\,dy}{\int\int c\,dx\,dy}, \tag{16}$$

which is plotted in Fig. 5. We observe that for the present viscosity ratio, after a brief initial transient the velocity levels off at a value of about 1.57. Subsequently the onset of the fingering instability causes it to rise to a peak of $U_d \approx 1.9$, which is close to the value of 2 for an immiscible circular bubble without surface tension in an infinite domain. Thereafter it drops rapidly. Around $t=2.1$, U_d rebounds slightly as a result of a merging process, before decreasing further.

A further quantity of practical interest, for example if chemical reactions between the two miscible fluids are to be considered, is the length of the interfacial region separating the two components. Chen and Meiburg[37] define an equivalent interfacial length $L(t)$ for miscible fluids as

$$L(t)=\int\int\left[\left(\frac{\partial c}{\partial x}\right)^2+\left(\frac{\partial c}{\partial y}\right)^2\right]^{1/2} dx\,dy. \tag{17}$$

For the present flow, the growth of this interfacial length is shown in Fig. 6. During the startup transient, when the droplet modifies its shape only weakly, the initial value $L=\pi$ is nearly maintained. Subsequently however, L grows rapidly to a maximum of more than three times its original value, which it reaches at about the time when U_d peaks. This reflects the vigorous fingering, which increases the contact area between the two fluids. Subsequently, the decay of the droplet structure into a pair of decaying fingers causes $L(t)$ to decrease, due to the diffusive decay of the concentration gradients.

One-dimensional profiles of the concentration averaged across the width of the Hele–Shaw cell, $c_a(x,t)$, can be employed to extract further global features of the flow, see Fig. 7. At $t=0.2$ the original droplet shape is still largely preserved. For later times, the c_a profiles near the trailing edge of the droplet display a largely monotonic character,

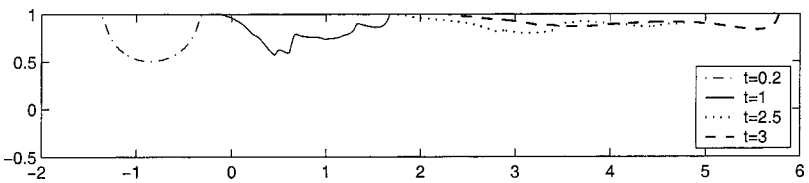

FIG. 7. Reference case: The average concentration profiles $c_a(x,t)$ at the same times as those shown in Fig. 2(a). The initially circular shape becomes increasingly stretched. While the rear of the droplet is governed by diffusive effects, the front is convectively dominated.

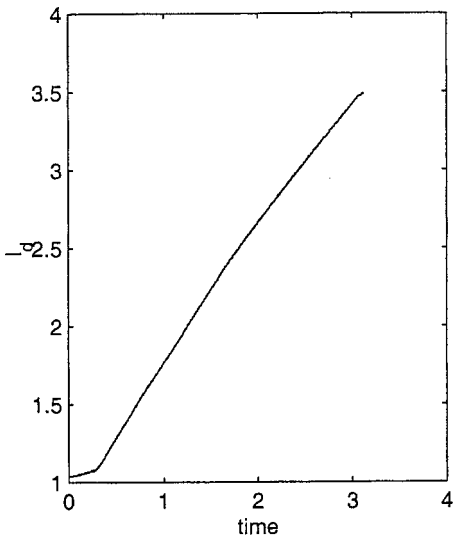

FIG. 8. Reference case: After an initial transient, the dispersed droplet length l_d grows nearly linearly with time.

indicating that diffusion is dominant. In contrast, near the front they resemble the convection dominated profiles observed earlier by Tan and Homsy[36] for nominally plane fronts, with plateau-like regions separated by steep gradients. A dispersed droplet length l_d can then be defined as the distance between the points at which c_a reaches a certain value close to one. Here, we take this value to be 0.98. Figure 8 shows that after the initial transient l_d increases approximately linearly with time, which reflects the continuous elongation of the droplet.

It should be mentioned that the above initial condition of a perfectly symmetric drop may appear somewhat artificial. For this reason, we also carried out simulations of slightly perturbed drops. While they evolved into an asymmetric shape, the general observations and conclusions arrived at above for the symmetric drop still hold. Furthermore, we will in the following limit ourselves to relatively large droplets whose initial diameter is half the width of the Hele–Shaw cell. While both Kopf-Sill and Homsy[6] as well as Tanveer[8,9] made interesting observations also for much smaller immiscible bubble sizes, we found such small miscible droplets to decay very rapidly at numerically accessible Pe values, so that not much could be learned from those simulations.

B. Displacements in the presence of Korteweg stresses

In the following, we will keep R and Pe at the values employed in the reference case, while exploring the effects of nonzero δ values. Hu and Joseph[33] pointed out that in Hele–Shaw flows the Korteweg stress constant δ has to have a negative value in order to avoid Hadamard instability, or ill-posedness of the problem. For miscible displacements in a capillary tube, Chen and Meiburg[28] employed negative values of δ and found them to be stabilizing, as they reduced the propagation velocity of the finger tip.

Figure 2(b) depicts the evolution of a droplet with $\delta = -10^{-6}$ for the same times as the reference case discussed above. While an exact value of the Korteweg stress constant between typical fluids is unknown at this time, the above value is suitable for demonstrating the nature of the influence that this stress can have in the flow. In comparison to the reference case, a clearly stabilizing effect is noticeable. While the fingering instability is not suppressed entirely, fewer and wider fingers evolve later in time. If the magnitude of the Korteweg stresses is further increased by setting $\delta = -10^{-5}$, the front of the drop becomes completely stabilized [Fig. 2(c)] and a tail evolves that resembles some of the shapes observed by Kopf-Sill and Homsy as well as Park *et al.* However, there is a fundamental difference between the miscible displacement and its immiscible counterpart, in that the immiscible flow can acquire a truly steady state, if viewed in a reference frame moving with the droplet. This possibility does not exist in the miscible case as a consequence of the actions of diffusion. At the leading edge of the drop, diffusion and strain can balance locally and thereby create a quasisteady state. However, such a balance cannot be achieved around the entire circumference of the drop, so that diffusion results in a continuous leakage of drop fluid into the wake.

A related effect of diffusion is that it spreads out the Korteweg stresses over a zone of finite thickness, whereas, at least in a continuum sense, the surface tension forces in the immiscible case are perfectly localized at the interface. Furthermore, since the magnitude of the Korteweg stresses depends on the square of the concentration gradient, the size of these stresses is to a large extent determined by the local balance of strain and diffusion. This influence is absent in the immiscible case. From these considerations, it is obvious that the analogy between the surface tension forces in an immiscible flow and the Korteweg stresses in a miscible flow has its limitations.

The local features of the velocity field thus prevent the formation of a well-defined, thin diffusion layer around the trailing section of the droplet. As a result, the Korteweg stresses are quite weak here, which renders them unable to maintain a quasisteady droplet shape in the same way as surface tension forces did in the investigations of Kopf-Sill and Homsy[6] and Park *et al.*[7] However, an impression of the time-dependent droplet shape can be obtained by drawing

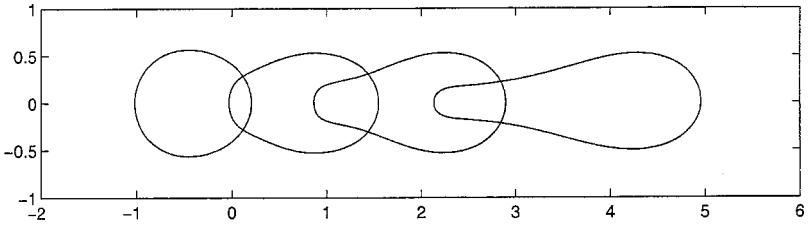

FIG. 9. Pe=2000, $R=-2.5$ and $\delta=-10^{-5}$. Shown are the droplet shapes at times $t=0.4$, 1.2, 2, and 3.2 by means of the $c=0.99$ contours. The formation of a droplet tail is clearly visible.

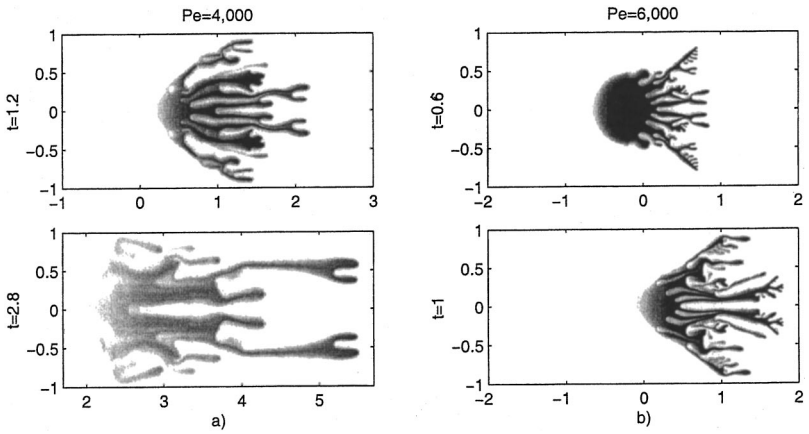

FIG. 10. Concentration contours for $R=-2.5$ and $\delta=0$: (a) Pe$=4000$, times $t=1.2$ and 2.8; (b) Pe$=6000$, times $t=0.6$ and 1. In the absence of Korteweg stresses, larger Pe values lead to increased fingering, and more frequent tip splitting events.

the $c=0.99$ contour at various times, cf. Fig. 9. The shape thus obtained again exhibits similarity with those observed by Kopf-Sill and Homsy as well as Park *et al.*

There is an interesting similarity between the effects of Korteweg stresses and diffusion in miscible flows, and those of a surfactant in immiscible ones. As Park *et al.* explain, if the bubble/droplet moves faster than the surrounding fluid, the surfactant will be swept to the rear of the droplet. As a result, surface tension forces will be strong at the leading edge of the droplet and much weaker near the trailing edge. For this reason, the balance of pressure forces requires the curvature at the tip of the tail to be much larger than at the droplet front, which results in the long and narrow tail shape observed by Kopf-Sill and Homsy and by Park *et al.* In miscible displacements with Kortewg stresses, the local balance of diffusion and strain creates a narrow concentration layer at the droplet's front, which results in locally strong Korteweg stresses. Near the rear of the droplet, the strain field does not counteract diffusion in the same way, so that a thick concentration layer results, with the result of locally weak Korteweg stresses. Applying Park's argument of a pressure balance across the droplet, these locally weak Korteweg stresses then necessitate a strongly curved concentration front, thereby resulting in a narrow tail with a pronounced tip.

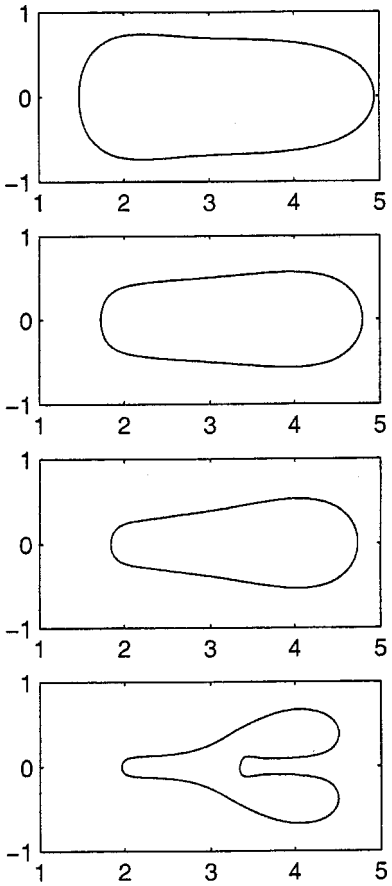

FIG. 11. $R=-2.5$ and $\delta=-10^{-5}$: Shown are the droplet shapes for Pe $=200$, 500, 1000, and 4000 at time$=3.2$. For low Pe values, the bubble falls into the elongated group, whereas at higher Pe values, there is an increased tendency towards tail formation.

C. Effects of Pe

For a certain droplet size, the value of Pe is directly proportional to the global displacement rate, and inversely proportional to the diffusion coefficient. As a result, the thickness of the concentration layer along the circumference of the drop, and with it the strength of the Korteweg stresses, depends on Pe. Higher Pe values generally lead to sharper concentration fronts, and consequently to larger Korteweg

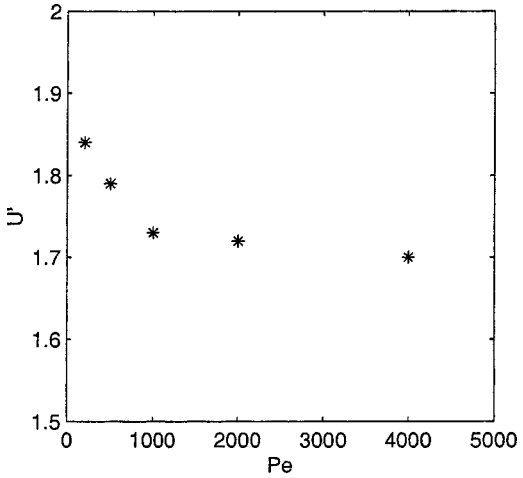

FIG. 12. $R=-2.5$ and $\delta=-10^{-5}$: The quasisteady droplet velocity U' is shown as a function of Pe. For large Pe, the droplets appear to move at an asymptotic velocity near 1.7.

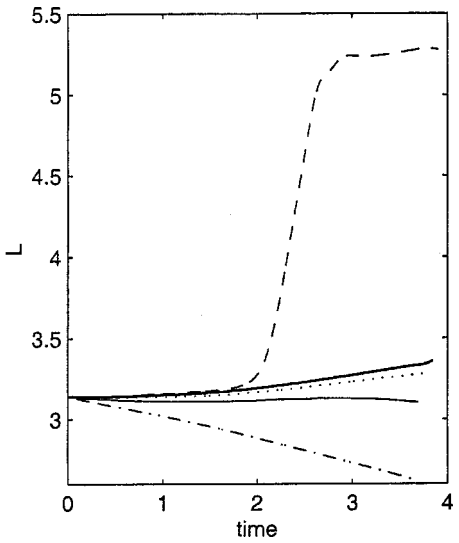

FIG. 13. $R=-2.5$ and $\delta=-10^{-5}$: The interfacial length L is shown as a function of time for Pe=200 (dash–dot), 500 (solid), 1000 (dot), 2000 (bold), and 4000 (dash).

stresses, which should stabilize the droplet. At the same time, sharper concentration fronts enhance the fingering instability along the droplet's leading edge, as shown in Fig. 10 for Pe=4000 and 6000, and $\delta=0$. This in turn results in a complex small scale structure of the advancing front, and in an increased growth rate for $L(t)$ for larger Pe values (Fig. 6). Consequently, the overall effect of Pe on miscible drops is difficult to predict, and it will depend on the value of the Korteweg stress constant δ.

Figure 11 shows concentration plots and droplet shapes (as defined by the $c=0.99$ contour) for $\delta=-10^{-5}$ and Pe values of 200, 500, 1000, and 4000 at $t=3.2$. We recognize the transition from an elongated droplet, see Kopf-Sill and Homsy,[6] to one with a pronounced tail as Pe grows. This indicates that, as the Korteweg stresses along the front of the droplet increase with Pe, a stronger curvature in the tail section evolves in order to achieve a pressure balance, in agreement with the argument by Park *et al.*[7] At the highest Pe value, the drop develops an instability at the front. This indicates that, at least for the present value of the Korteweg stress constant, the destabilizing effects of higher Pe outweigh the stabilizing ones.

For these droplets with stable leading edges, it is useful to define an alternate quasisteady propagation velocity U' as the velocity with which the $c=0.5$ concentration contour at the droplet tip propagates. Figure 12 shows that this quasisteady velocity U' *decreases* with increasing Pe, towards what appears to be an asymptotic value near 1.7.

The dependence of the interfacial length $L(t)$ on Pe is depicted in Fig. 13. The decay of L with time for Pe=200 reflects the fact that for strong diffusion our measure of an effective interfacial length is of limited use. However, for larger Pe values we notice a more rapid growth of the interfacial length, which results from both the tip splitting as well as the tendency to form a tail.

D. Effects of the viscosity parameter *R*

The interplay of the viscosity ratio with the Korteweg stresses is even more difficult to predict than that of Pe, as R affects the steepness of the concentration gradients, and thereby the Korteweg stresses, only indirectly. It does so mainly by influencing the stability properties of the drop. In the absence of Korteweg stresses, an increased viscosity contrast generally renders the drop more unstable (Fig. 14). Thus an enhanced production of small scales results, which leads to locally steeper concentration gradients. Interestingly, when considering more viscous drops embedded in a less viscous environment we never observed an instability localized along the trailing edge of the drop, not even for the large values of $R=5$ and Pe=4000, which create a strongly unfavorable mobility ratio. A possible explanation may be that instability waves originating near the rear of the droplet are swept towards more stable regions of the interface by the faster surrounding fluid. Furthermore, their wavelength would be increased during this process, as a result of the local strain field. However, similar arguments should then hold for the instability waves originating near the tip of the droplet when the droplet fluid is the less viscous one. A more likely explanation may be found in the stabilizing influence of the shear across the interface, as analyzed by Rogerson and Meiburg.[45,46]

Even in the absence of an instability, the Korteweg stresses affect the droplet propagation velocity, and thereby the strain field along the surface of the drop, which in turn influences the steepness of the concentration gradients. Figure 15 shows the droplet shapes for the viscosity ratios $R=-1$, -2, and -3.5, and $\delta=-10^{-5}$. A larger viscosity contrast is seen to enhance the droplet migration velocity U', cf. Fig. 16. It thereby steepens the concentration field

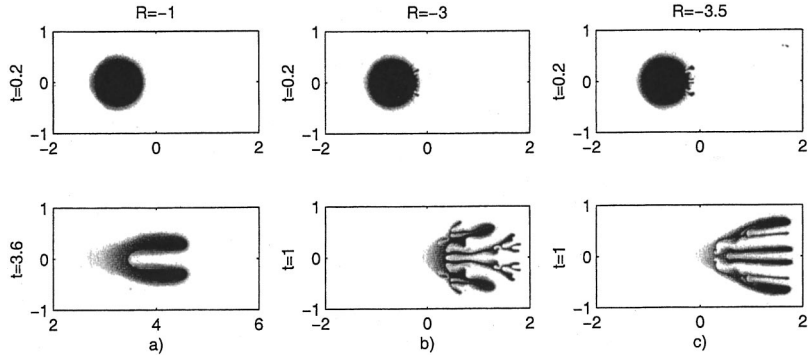

FIG. 14. Pe=2000 and $\delta=0$: Concentration contours for (a) $R=-1$, (b) $R=-3$, and (c) $R=-3.5$. In the absence of Korteweg stresses, a higher mobility contrast renders the flow more unstable.

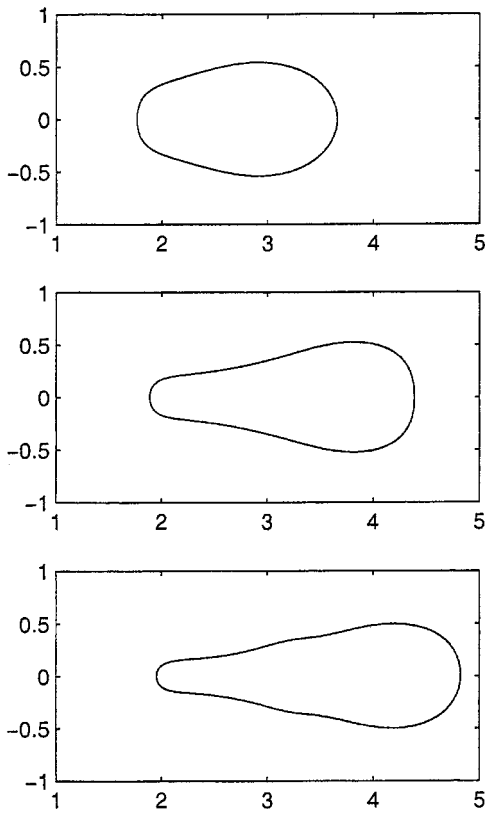

FIG. 15. Pe=2000 and $\delta=-10^{-5}$: Droplet shapes for $R=-1$, -2, and -3.5 at $t=3.2$. Larger mobility ratios result in an increased tendency towards tail formation.

near the leading edge, which locally enhances the Korteweg stresses, so that the need to balance the pressure forces results in a longer, narrower tail, as seen in Fig. 15. It is difficult to compare the computational observations on the influence of R with either theory or experiments, since all of the investigations by Tanveer, Kopf-Sill, and Homsy, and by Park *et al.* considered inviscid or essentially inviscid bubbles.

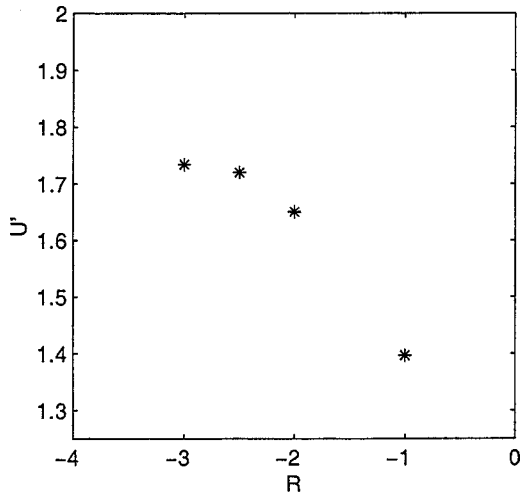

FIG. 16. Pe=2000 and $\delta=-10^{-5}$: Quasisteady droplet velocity U' as function of R. Larger viscosity contrasts result in higher droplet velocities.

IV. DISCUSSION AND CONCLUSIONS

The above simulations are intended to clarify the displacement dynamics, in a porous medium, of a drop embedded in a miscible environment. In the absence of Korteweg stresses, such drops initially show a behavior in line with earlier investigations of unstable planar fronts. For larger Pe values and viscosity contrasts, they become increasingly unstable and develop more and more fine scale structure. In this process, interfacial length is generated at a faster rate. Sooner or later, however, these unstable drops evolve into a small number of fading fingers, as a result of the limited supply of less viscous fluid.

Our main interest focused on the influence of nonconventional, so-called Korteweg stresses that act in regions of steep concentration gradients. We accounted for those stresses by basing our simulations on a set of augmented Hele–Shaw equations as proposed by Hu and Joseph.[33] These stresses were seen to have a globally stabilizing effect on the drop behavior. However, important differences were observed between the action of these Korteweg stresses and those of surface tension in an immiscible displacement. Korteweg stresses depend on the local concentration gradient field, so that the effective net force across the miscible interface region is not just a function of the drop's geometry, but also of the velocity gradient tensor. In all of our simulations, the drop moved faster than the surrounding fluid, so that a local compression region forms at the leading edge of the drop, which in turn results in a steep concentration gradient and large Korteweg stresses. Around the rear of the drop, the diffusion layer is much thicker, and consequently the Korteweg stresses are smaller. A balance of the pressure forces acting on the drop then requires a region of very strong curvature at the trailing edge, which in turn results in the formation of a tail. In this sense, the Korteweg stresses cause droplet behavior similar to that seen in the immiscible flows with surfactants studied by Park *et al.*[7] and, presumably, Kopf-Sill and Homsy.[6]

The dimensionless flow rate in the form of Pe is seen to affect the drop's behavior in complex ways. On one hand, the sharper concentration layer renders the drop more unstable with respect to the viscous fingering instability, but at the same time it results in larger stabilizing Korteweg stresses. Which one of these effects wins out must depend on the size of the Korteweg stress constant. Perhaps the competition and balance of these two effects could be exploited to evaluate the magnitude of this constant, which is so far unknown. However, it is to be kept in mind that the form of the Korteweg stress terms proposed by Hu and Joseph,[33] on which the present investigation is based, has not yet been derived from first principles, and that their validation remains an important problem.

ACKNOWLEDGMENTS

Support through the Republic of China NSC Research Grant No. 89-2212-E-212-036, by NASA, the Department of Energy, and the Petroleum Research Fund is gratefully acknowledged.

[1]G. Homsy, ''Viscous fingering in porous media,'' Annu. Rev. Fluid Mech. **19**, 271 (1987).
[2]Y. Yortsos, ''Instabilities in displacement processes in porous media,'' J. Phys.: Condens. Matter **2**, SA443 (1990).
[3]K. V. McCloud and J. V. Maher, ''Experimental perturbations to Saffman–Taylor flow,'' Phys. Rep. **260**, 139 (1995).
[4]W. Eck and J. Siekmann, ''Bubble motion in a Hele–Shaw cell, a possibility to study 2-phase flows under reduced gravity,'' Ing. Arch. **47**, 153 (1978).
[5]T. Maxworthy, ''Bubble formation, motion and interaction in a Hele–Shaw cell,'' J. Fluid Mech. **173**, 95 (1986).
[6]A. Kopf-Sill and G. Homsy, ''Bubble motion in a Hele–Shaw cell,'' Phys. Fluids **31**, 18 (1988).
[7]C.-W. Park, S. Maruvada, and D.-Y. Yoon, ''The influence of surfactant on the bubble motion in Hele–Shaw cells,'' Phys. Fluids **6**, 3267 (1994).
[8]S. Tanveer, ''The effect of surface tension on the shape of a Hele–Shaw cell bubble,'' Phys. Fluids **29**, 3537 (1986).
[9]S. Tanveer, ''New solutions for steady bubbles in a Hele–Shaw cell,'' Phys. Fluids **30**, 651 (1987).
[10]S. Tanveer and G. Saffman, ''Stability of bubbles in a Hele–Shaw cell,'' Phys. Fluids **30**, 2624 (1987).
[11]G. I. Taylor and P. G. Saffman, ''A note on the motion of bubbles in a Hele–Shaw cell and porous medium,'' J. Mech. Appl. Math. **12**, 265 (1959).
[12]J. McLean and P. G. Saffman, ''The effect of surface tension on the shape of fingers in a Hele–Shaw cell,'' J. Fluid Mech. **102**, 455 (1981).
[13]F. B. Bretherton, ''The motion of long bubbles in tubes,'' J. Fluid Mech. **10**, 166 (1961).
[14]C.-W. Park and G. M. Homsy, ''Two-phase displacements in Hele–Shaw cells: Theory,'' J. Fluid Mech. **139**, 291 (1984).
[15]E. Meiburg, ''Bubbles in a Hele–Shaw cell: Numerical simulation of three-dimensional effects,'' Phys. Fluids A **1**, 938 (1989).
[16]D. Korteweg, ''Sur la forme que prennent les équations du mouvement des fluides si l'on tient compte des forces capillaires causées par des variations de densité,'' Arch. Neel. Sci. Ex. Nat. **II**, 6 (1901).
[17]D. Joseph, ''Fluid dynamics of two miscible liquids with diffusion and gradient stresses,'' Eur. J. Mech. B/Fluids **9**, 565 (1990).
[18]M. Kojima, E. J. Hinch, and A. Acrivos, ''The formation and expansion of a toroidal drop moving in a qiescent fluid,'' Phys. Fluids **27**, 19 (1984).
[19]G. Galdi, D. Joseph, L. Prezisi, and S. Rionero, ''Mathematical problems for miscible, incompressible fluids with Korteweg stresses,'' Eur. J. Mech. B/Fluids **10**, 253 (1991).
[20]D. Joseph and Y. Renardy, *Fundamentals of Two-Fluid Dynamics* (Springer, Berlin, 1962), Part II.
[21]D. Joseph, A. Huang, and H. Hu, ''Non-solenoidal velocity effects and Korteweg stresses in simple mixture of incompressible liquids,'' Physica D **97**, 104 (1996).
[22]G. Quinke, ''Die Oberflaechenspannung an der Grenze von Alcohol mit waesserigen Salzloesungen,'' Ann. Phys. (Leipzig) **1902**, 4 (1902).
[23]H. Freundlich, *Colloid and Capillary Chemstry* (Mathuen, London, 1926).
[24]P. G. Smith, T. G. M. van De Ven, and S. G. Mason, ''The transient interfacial tension between two miscible fluids,'' J. Colloid Interface Sci. **80**, 302 (1981).
[25]P. Petitjeans and T. Maxworthy, ''Miscible displacements in capillary tubes. Part 1: Experiments,'' J. Fluid Mech. **326**, 37 (1996).
[26]G. I. Taylor, ''Deposition of a viscous fluid on the wall of a tube,'' J. Fluid Mech. **10**, 161 (1961).
[27]C.-Y. Chen and E. Meiburg, ''Miscible displacements in capillary tubes. Part 2: Numerical simulations,'' J. Fluid Mech. **326**, 57 (1996).
[28]C.-Y. Chen and E. Meiburg, ''The dynamics of miscible interfaces and the effects of Korteweg stresses,'' in Proceedings of the Seventh (ROC) National Computational Fluid Dynamics Conference, 2000.
[29]H. Davis, ''A theory of tension at a miscible displacement front,'' in *IMA Volumes in Mathematics and its Applications* (Springer, Berlin, 1988), p. 11.
[30]P. Kurowski and C. Misbah, ''A non-standard effect of diffusion on a fictitious front between miscible fluids,'' Europhys. Lett. **29**, 309 (1994).
[31]P. Petitjeans, ''Une tension de surface pour les fluides miscibles,'' C. R. Acad. Sci., Paris, Ser. IIb **322**, 673 (1996).
[32]P. Petitjeans and P. Kurowski, ''Fluides non miscibles/fluides miscibles: des similitudes interessantes,'' C. R. Acad. Sci. Paris, Ser. IIb **325**, 587 (1997).
[33]H. Hu and D. Joseph, ''Miscible displacement in a Hele–Shaw cell,'' Z. Angew. Math. Phys. **43**, 626 (1992).
[34]J. Fernandez, P. Kurowski, P. Petitjeans, and E. Meiburg, ''Density-driven, unstable flows of miscible fluids in a Hele–Shaw cell,'' submitted to J. Fluid Mech.
[35]P. Petitjeans, C.-Y. Chen, E. Meiburg, and T. Maxworthy, ''Miscible quarter five-spot displacements in a Hele–Shaw cell and the role of flow-induced dispersion,'' Phys. Fluids **11**, 1705 (1999).
[36]C. T. Tan and G. M. Homsy, ''Simulation of nonlinear fingering in miscible displacement,'' Phys. Fluids **31**, 1330 (1988).
[37]C.-Y. Chen and E. Meiburg, ''Miscible porous media displacements in the quarter five-spot configuration. Part 1: The homogeneous case,'' J. Fluid Mech. **371**, 233 (1998).
[38]C.-Y. Chen and E. Meiburg, ''Miscible porous media displacements in the quarter five-spot configuration. Part 2: Effect of heterogeneities,'' J. Fluid Mech. **371**, 269 (1998).
[39]M. Ruith and E. Meiburg, ''Miscible rectilinear displacements with gravity override. Part 1: Homogeneous porous medium,'' J. Fluid Mech. **420**, 225 (2000).
[40]E. Camhi, E. Meiburg, and M. Ruith, ''Miscible rectilinear displacements with gravity override. Part 2: Heterogeneous porous media,'' J. Fluid Mech. **420**, 225 (2000).
[41]S. Lele, ''Compact finite difference schemes with spectral-like resolution,'' J. Comput. Phys. **103**, 16 (1992).
[42]A. Wray, ''Minimal storage time-advancement schemes for spectral methods'' (unpublished).
[43]C. Canuto, M. Y. Hussaini, A. Quarteroni, and T. A. Zang, *Spectral Methods in Fluid Mechanics* (Springer, Berlin, 1988).
[44]E. Meiburg and C.-Y. Chen, ''High-accuracy implicit finite difference simulations of homogeneous and heterogeneous miscible porous media flows,'' SPE J. **5**, 2 (2000).
[45]A. Rogerson and E. Meiburg, ''Shear stabilization of miscible displacement process in porous media,'' Phys. Fluids A **5**, 1344 (1993).
[46]A. Rogerson and E. Meiburg, ''Numerical simulation of miscible displacement processes in porous media flows under gravity,'' Phys. Fluids A **5**, 2644 (1993).